Appl. Phys. B 65, 81–91 (1997)

Applied Physics B Lasers and Optics

Measurement of vibrational energy transfer of OH ($A^2\Sigma^+$, $v' = 1 \rightarrow 0$) in low-pressure flames

A.T. Hartlieb, D. Markus, W. Kreutner, K. Kohse-Höinghaus

Universität Bielefeld, Fakultät für Chemie, Physikalische Chemie 1, Universitätsstraße 25, D-33615 Bielefeld, Germany
(E-mail: KKH@CHEP118.UNI-BIELEFELD.DE)

Received: 9 September 1996/Revised version: 6 January 1997

Abstract. Vibrational energy transfer (VET) and electronic quenching of OH ($A^2\Sigma^+$) was measured in a low-pressure H_2/O_2 flame for three rotational levels of OH ($v' = 1$). Rate coefficients for collisions with H_2O and N_2 were determined. At 1600 K, k_{VET} (N_2) is (in 10^{-11} cm^3s^{-1}) 10.1 ± 2, 6.1 ± 1.8, and 3.8 ± 1.3 for $N' = 0$, 5, and 13, respectively. The k_{VET} (H_2O) is $\leq 1.1 \pm 1.8$. The k_Q (N_2) is $\leq 2.4 \pm 8$ for both vibrational levels. The k_Q (H_2O) in $v' = 1$ is 59.1 ± 6.5, 54.7 ± 6.4, and 54.9 ± 6.6 for $N' = 0$, 5, and 13, respectively, and, determined indirectly, 74.6 ± 10.4, 70.6 ± 10.3, and 63.4 ± 7.3 for $N' = 0$, 5, and 13 in $v' = 0$. A multi-level model of OH population dynamics, which is being developed for the quantitative simulation of experimental LIF spectra, was extended to include VET. It was attempted to simulate state-to-state-specific VET coefficients for N_2 collisions. From these simulations it appears that angular momentum conservation does not determine the N dependence of the vibrational relaxation step.

PACS: 33.50.-j; 34.50.Ez; 82.40

The hydroxyl radical (OH) plays an important role in both combustion and atmospheric chemistry. Laser-induced fluorescence (LIF) is a widely used method for the detection of OH in flames and other highly reactive media (see e.g. [1] for a recent review). If a quantitative relation between measured LIF signal and OH number density is to be established, a fairly detailed knowledge of molecular energy transfer processes is required. The three most important ones are electronic quenching, rotational energy transfer (RET) and vibrational energy transfer (VET). In this paper, emphasis will be put on VET and quenching of OH under flame conditions. Several authors [2–7] investigated the VET process of OH (A) near room temperature and derived rate coefficients for a number of collider species. For elevated temperatures, the only quantitative measurements that we are aware of are shock tube data from Paul [8] at $T = 1900$ K and 2300 K. He employed N_2, O_2, CO, CO_2, NO, Ar, Kr, and Xe for collider species and always excited the $N' = 5$ level of OH (A).

Quenching and energy transfer processes can be viewed as collisional effects which compete with the radiative decay of the excited state. Their respective efficiencies are strongly dependent on the collision partners (i.e. chemical composition of the bath gas), collision frequency (i.e. pressure) and the velocity of collision partners (i.e. temperature). Quenching reduces the number of molecules in the excited state after electronic excitation, whereas RET and VET result in a redistribution over the rotational and vibrational ensemble of energy levels, respectively. Under typical flame conditions, VET is the slower process. Hence VET is, on average, both preceded and followed by RET. The experimentally detectable population in a particular rotation-vibrational level is the net result of many different possible sequences of state-changing collisions, with various paths leading from the initially laser-populated state to the OH energy level whose fluorescence is finally observed. This makes it difficult to disentangle rotational redistribution from vibrational relaxation. Measurements in a flame pose some additional problems for data evaluation, because there is always more than one collider species present (up to 7 had to be considered in the present analysis), and the large number of rotational levels populated at flame temperatures results in spectral overlap between the vibrational bands in the emission spectra. Therefore, experimental measurements need to be supplemented by numerical modelling studies, where the state-to-state dynamics of the OH radical can be simulated. The ultimate goal for this model development is the capability to predict, as quantitatively as possible, the experimental LIF spectra which are obtainable with the various excitation/detection schemes. This will be very helpful for the selection of an optimized measurement strategy for a given set of boundary conditions. In such a model, the effects of different assumptions regarding selection rules and N dependence of rate coefficients etc. can be studied. Usually, a rate equations approach for the time dependence of the various populations is used. Several models with varying degrees of sophistication are described in the literature [9–14].

In this work, we present measurements of OH vibrational energy transfer as well as quenching at elevated temperatures in low-pressure H_2/O_2 flames. Three different rotational lev-

els in the $A^2\Sigma^+(v'=1)$ state were initially populated. Rate coefficients for VET and quenching by H_2O and N_2 were derived, and trends regarding the N dependence of VET were observed. The LASKIN simulation code [13, 14] was extended to include VET between $v'=1$ and $v'=0$, and some attempts were made to find adequate models for rotational-state-to-state-specific VET coefficients.

1 Experimental

The experimental setup employed in this study was very similar to the one fully described in a previous study [15]; only the most important features will be discussed here. The laser source consisted of a tunable Nd:YAG/dye-laser system with ≈ 5 nsec pulse duration which produced light around 281 nm for excitation in the OH A-X 1–0 band. A sintered porous plug burner (McKenna Instruments, 60 mm diameter) was operated at 50 mbar with a stoichiometric mixture of H_2 and O_2. In comparison with the operating conditions reported in [15], the pressure was doubled. This reduces the concentration of educts and intermediate species like H and O atoms at the measurement location, 48 mm above the porous plug, and thus facilitates data interpretation. Three different flames were investigated: (a) A "pure" H_2/O_2 flame with gas flows of 4.67 and 2.35 slm; (b) one diluted with He (H_2/O_2/He : 2.37/1.40/2.93 slm); and (c) one with added N_2 ($H_2/O_2/N_2$: 2.37/1.39/3.31 slm). Hereafter, they will be referred to as the H_2/O_2, the helium-doped, and the nitrogen-doped flame, respectively.

Both broadband and narrowband detection channels were employed. Broadband, i.e. spectrally integrated, LIF was detected both for temperature measurement by OH excitation spectra and for measuring the time-resolved fluorescence signals for the determination of VET and quenching coefficients. For the excitation spectra, a suitable combination of colored glass and interference filters was used to select the OH 0–0 and 1–0 bands. For measuring the time-resolved fluorescence signal, a small monochromator (Acton Research ARC 275, equipped with 600 grooves/mm and 1800 grooves/mm gratings) was used to isolate a rectangular spectral bandpass of 18.05 nm FWHM (for measuring the 1–0 and 1–1 bands) and 5.7 nm FWHM (for the 0–0 band), respectively. Narrowband, i.e. spectrally resolved fluorescence signals were measured with a $f = 640$ mm monochromator (Jobin Yvon HR640) equipped with a 2400 grooves/mm grating. For the time-resolved signals, a fast photomultiplier tube (Hamamatsu H3378-01) was employed in conjunction with a transient digitizer (Tektronix R7912). The excitation spectra and the narrowband signals were detected using a high-gain photomultiplier tube (Valvo XP2020Q) and processed with a gated integrator/boxcar averager (Stanford Research Systems SR250). Usually a gate width of 100 ns was employed and the signal average of 30 pulses was taken.

2 Results and data analysis

This section is organized as follows. After a brief presentation of the raw data, the analysis proceeds in three steps: first a determination of total removal rates for the two vibrational levels; next, species-specific coefficients are derived for N_2 and H_2O; and finally, the possibility of modeling state-to-state-specific rate coefficients for the flames under investigation is discussed. The discussion will show that with every new step, additional assumptions and approximations need to be invoked.

2.1 Measurements

The primary data obtained from the measurements are spectrally resolved, time-integrated LIF spectra of the 0–0 and 1–1 band region, covering the range from 306 to 325 nm (cf. Fig. 1a and 1b); and time-resolved "transient" fluorescence intensities (cf. Fig. 2), where the signal from one vibrational state was spectrally integrated over a wavelength range corresponding to the non-overlapped part of the 0–0 band (for measuring the $v'=0$ population) and the 1–1 or 1–0 band, respectively. Both LIF spectra and time-resolved signals were measured in each flame for three different OH excitation lines of the 1–0 A-X band, namely the $P_1(1)$, $Q_1(5)$ and $R_1(12)$ lines [16]. This corresponds to populating the F_1 levels with $N'=0$, 5 and 13 in OH (A, $v'=1$).

Figures 1a and 1b show the LIF spectra with excitation of the $Q_1(5)$ line from the H_2/O_2 and N_2-doped flames. As a qualitative picture, it can be seen that the relative signal strength in the 0–0 band region is stronger for the N_2-doped flame. The P, Q and R branch lines originating from the directly pumped level in $v'=1$ are marked (+). It can be seen that there is no obvious preference in populating the same N level in $v'=0$ (marked (×)), in full agreement with the room-temperature findings of e.g. Lengel et al. [2]. Also, there is no evidence for selectivity of F_1 versus F_2 doublet components in the VET step. Figure 2 shows the time-resolved signals measured in the N_2-doped flame, again for the $Q_1(5)$ excitation line. It is clearly visible that the signal of $v'=0$ has a larger rise time and delayed onset, because this level first has to be populated by collisions. In measuring the time-resolved signal from the 0–0 band, particular care must be taken to make sure that the small monochromator's bandpass does not transmit a portion of the 1-1 band, and vice versa (cf. Sect. 2.3 below). Selection of the monochromator position is less critical for the 1–0 band, but here the signal intensities are smaller.

The general procedure for extracting rate coefficients from that kind of raw data comprises several steps. From the LIF spectra, a quantitative measure must be derived for the amount of population transferred from the initially laser-pumped level $v'=1$ into $v'=0$. To do so, the problem of spectral overlap between the bands must be addressed. The time-resolved signals can then be evaluated, first in terms of total removal rates. For this, the corresponding expressions are derived from the differential equations which describe the system, and eventually fitted to the experimental curves. To convert these total removal rates to collider-specific rate coefficients, additional information about the gas composition of the flame is required. The discussion will show that the VET and quenching contributions of several minor constituents in the flame gases have to be accounted for in this analysis, hence their concentrations must be determined. The different steps will now be discussed in some detail.

The observable fluorescence signal is the net result of competition between radiative decay, quenching, rotational

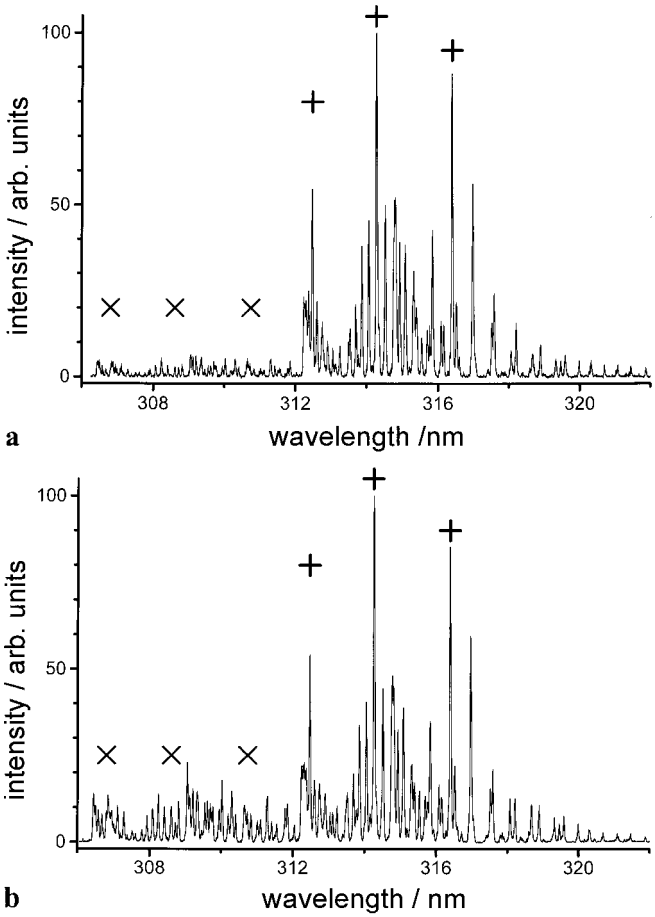

Fig. 1a,b. Laser-induced fluorescence spectra from the H_2/O_2 flame (**a**)and the N_2-doped flame (**b**). The 1–1 band head is at 312.2 nm. The crosses + mark the position of lines originating from the directly pumped rotational level in $v' = 1$ ($Q_1(5)$ excitation); the × mark the corresponding regions in the $v' = 0$ state. Note the different relative amplitudes for the 0–0 and 1–1 bands in the two flames

and vibrational relaxation. At the measurement location in the flame, more than one species will collide with the OH radical, hence the flame composition must be known, and the rate coefficients for quenching, RET and VET for all relevant collision partners must be examined. Flame compositions were calculated using the CHEMKIN code [17] for one-dimensional flames. The input parameters required for this calculation are the gas flow velocities and the axial temperature profile of the flame. The latter was determined from a series of excitation scans in the 1–0 band of OH, using procedures that were described previously [15]. In Table 1, temperatures and the resulting flame compositions at the measurement location are given. Note that the educts H_2 and O_2 as well as the intermediate radicals H, O, and OH are lumped together as a "residual" component with 11.9 to 18.1 mole-% concentration.

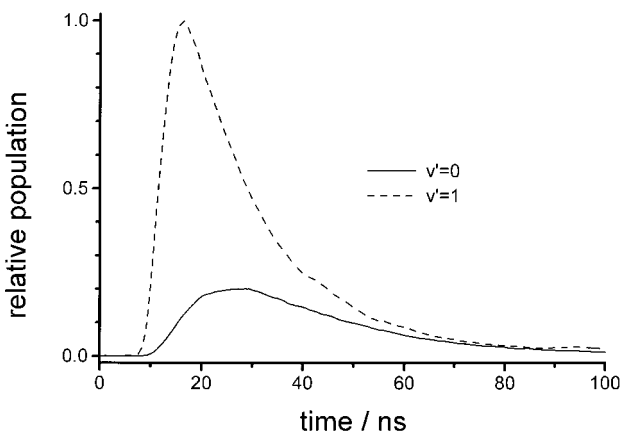

Fig. 2. Time-resolved, spectrally integrated fluorescence signals from the $v' = 1$ and $v' = 0$ level in the N_2-doped flame. Excitation line: $Q_1(5)$ in $v' = 1$. The area under the curves is normalized and corresponds to the ratio of time-integrated populations in $v' = 1$ and 0 [cf. (10)]

2.2 Differential equation system

A kinetic rate equation system was used in the data analysis. The time-dependent population in the $v' = 1$ and $v' = 0$ levels, $N_1(t)$ and $N_0(t)$, is described by

$$\frac{\mathrm{d}N_1(t)}{\mathrm{d}t} = \tau_1^{-1} N_1(t)\,, \tag{1}$$

$$\frac{\mathrm{d}N_0(t)}{\mathrm{d}t} = V_{10} N_1(t) - \tau_0^{-1} N_0(t)\,, \tag{2}$$

with

$$\tau_1^{-1} = \tau_{1,\mathrm{RAD}}^{-1} + n \sum_i x_i (k_{\mathrm{Q}_1,i} + k_{\mathrm{VET},i})\,, \tag{3}$$

$$V_{10} = n \sum_i x_i k_{\mathrm{VET},i}\,, \tag{4}$$

and

$$\tau_0^{-1} = \tau_{0,\mathrm{RAD}}^{-1} + n \sum_i x_i k_{\mathrm{Q}_0,i} \tag{5}$$

Here, n is the total number density; x_i is the mole fraction of species i; $k_{\mathrm{Q}_0,i}$ and $k_{\mathrm{Q}_1,i}$ are the rate coefficients of species i for electronic quenching of OH in the $v' = 0$ and $v' = 1$ states, respectively. $k_{\mathrm{VET},i}$ is the rate coefficient of species

Table 1. Calculated flame composition (mole fractions, in percent) at the measurement location, calculated with the CHEMKIN flame code for 50 mbar. Temperature as determined from OH LIF excitation scans. In the text, the sum of rows (a) to (e) is also referred to as a "residual" component

flame:	H_2/O_2	He-doped	N_2-doped
collider species:			
(a) H_2	6.84	2.55	3.04
(b) H	2.83	2.16	2.90
(c) O	0.89	0.79	1.05
(d) O_2	4.66	5.28	5.14
(e) OH	2.89	1.11	1.33
(a+b+c+d+e = "residual")	(18.11)	(11.89)	(13.46)
(f) H_2O	81.89	36.69	32.78
(g) He	0.00	51.43	0.00
(h) N_2	0.00	0.00	53.76
temperature/K	1920	1520	1600

i for vibrational transfer from $v' = 1$ to $v' = 0$, and $\tau_{0,\mathrm{RAD}}^{-1}$ and $\tau_{1,\mathrm{RAD}}^{-1}$ are the radiative transition rates of the two vibrational states. It is clear that the chemical composition must be known to determine species-specific rate coefficients. Note that RET is not taken into account at this stage, since it does not change the overall population of a vibrational level. This means that the V_{10} rate will be somewhat "contaminated" by contributions from rotational levels other than the originally pumped one, even though it was attempted to minimize this effect (cf. Sect. 2.4 below). Another source of systematic error is the endoergetic energy back transfer ($v' = 0 \rightarrow v' = 1$), which was ignored to simplify the analysis. This may affect the results at very high temperatures (for OH, one vibrational quantum is of the order of kT for $T = 4300$ K). In their shock tube study, Paul et al. [18] observed an emission from $v' = 1$, after excitation to $N' = 2$ or $N' = 5$ in $v' = 0$, which at 2300 K corresponded to at most 2–4% of the population in the A state. At the lower temperatures employed in our study, it is safe to assume that this fraction will be lower still and can thus be ignored. Equations (1) and (2) can be solved for $N_1(t)$ and $N_0(t)$:

$$N_1(t) = N_1(t_0) \exp\left(-\frac{t - t_0}{\tau_1}\right) \tag{6}$$

$$N_0(t) = \left[\frac{V_{10} N_1(t_0)}{\tau_0^{-1} - \tau_1^{-1}} \left[\exp[-(t - t_0)(\tau_1^{-1} - \tau_0^{-1})] - 1\right] + N_0(t_0)\right] \exp\left(-\frac{t - t_0}{\tau_0}\right) \tag{7}$$

To determine V_{10}, one can also integrate (2), yielding

$$V_{10} = \frac{N_0(t) - N_0(t_0) + \tau_0^{-1} \int_{t_0}^{t} N_0(t')\,\mathrm{d}t'}{\int_{t_0}^{t} N_1(t')\,\mathrm{d}t'}\,. \tag{8}$$

For $N_0(t_0) = N_0(t = \infty) = 0$ (which holds for times before the start of the laser pulse and after complete decay of the fluorescence signal), (8) simplifies to

$$V_{10} = \tau_0^{-1} \cdot c_\mathrm{p} \tag{9}$$

where the factor c_p is the ratio of time-integrated populations in $v' = 0$ and $v' = 1$:

$$c_\mathrm{p} = \frac{\int N_0(t)\,\mathrm{d}t}{\int N_1(t)\,\mathrm{d}t} \tag{10}$$

Hence, the magnitude of c_p is an indication of the efficiency of VET at a given combination of flame composition and excitation line. This population factor c_p can be determined from the relative signal intensities of spectrally resolved measurements.

2.3 Population ratios

A difficulty in determining this ratio of populations arises in a high-temperature environment. Several spectral lines of the 0–0 band, particularly P and Q branch lines originating from high rotational levels, are overlapped by lines in the 1–1 band. In the simulated spectrum [19] of Fig. 3, the contributions of lines originating from $v' = 0$ and $v' = 1$ are shown separately. Quite clearly, a substantial fraction of the signal from $v' = 0$ will be masked by the intense emission from the directly laser-pumped level $v' = 1$. This fraction is not known *a priori*; to determine it, the population distribution should be known.

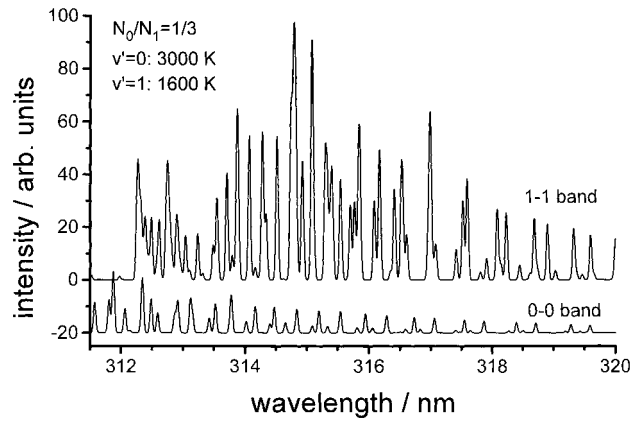

Fig. 3. Simulated OH LIF spectra for $v' = 1$ and $v' = 0$ emission, assuming a population ratio of $3 : 1$ ($v' = 1 : v' = 0$). Rotational temperature was 1600 K in $v' = 1$ (flame temperature) and 3000 K in $v' = 0$ (apparent temperature after VET). The bandhead of the 1–1 band is at 312.2 nm

As was first noted in a room temperature study by Lengel et al. [2], this rotational distribution within $v' = 0$, after the vibrational relaxation step, is rather similar to a thermal one, but with an apparent "temperature" much higher than the real gas temperature. For the purpose of estimating the fraction of the 0-0 band signal hidden by the 1–1 band emission, the rotational distribution can be approximately described by such an apparent temperature. In a very recent discharge flow reactor study at room temperature, Williams et al. [7] analyzed the OH rotational distribution within $v' = 0$ after VET. They found non-thermal population distributions which can loosely be thought of as being superpositions of two different Boltzmann distributions with very different temperatures. For the analysis of our flame data, the simpler assumption of a single, higher temperature was found to be a sufficiently good approximation. In spite of some irregular peak heights (particularly in the spectra with excitation of the $R_1(12)$ line) that could not yet be fully analyzed, the distribution in the time-integrated LIF spectra resembles a thermal distribution with a substantially elevated rotational temperature. (To illustrate this point, the rotational temperature for the simulated spectra in Fig. 3 was chosen to be much higher in $v' = 0$ than in $v' = 1$.) With the assumption that this distribution persists also for the high rotational levels in $v' = 0$, one can calculate the fraction of the 0-0 band emission which is hidden under the 1–1 band lines, and appropriately correct the relative signal intensity. The validity of this assumption could be roughly checked for the N_2-doped flame by determining peak intensity ratios for the 0–0 $P_1(15)$ and $P_1(5)$ lines; the former one appears near 316.6 nm, without overlap from 1–1 band transitions. The resulting two-line-temperatures were consistent with the apparent temperature derived from the non-overlapped part of the 0–0 band. A temperature fitting routine [20] was used to extract these apparent temperatures from the 306–312 nm spectral range, where the

0–0 band is not overlapped by other lines. The same trend was observed in all three flames: The apparent temperature in $v' = 0$ increased with the rotational quantum number of the directly laser-populated level. In the case of the nitrogen-doped flame with a gas temperature of 1600 K, the apparent temperatures were 2150 K ($P_1(1)$ excitation), 2500 K ($Q_1(5)$ excitation) and 4900 K ($R_1(12)$ excitation).

In Fig. 4, the temperature dependence of the correction factor f_{hidden} is shown for the 1500–5000 K range. Note that this correction ($I_{\text{true}} = I_{\text{measured}}(1 + f_{\text{hidden}})$) can be quite substantial, amounting to about 50% for the above-mentioned apparent temperature of 4900 K in the case of the $R_1(12)$ excitation line. To convert from relative signal intensities (both time-resolved and time-integrated signals) to populations, an effective Einstein A coefficient was calculated for the two vibrational levels using the values tabulated in [21] and rotational state populations. In the case of the 0–0 band, the populations corresponding to the apparent temperature were used. For the 1–1 band, time-integrated populations were calculated using the LASKIN code [13, 14, 22] to simulate RET within $v' = 1$. Figure 5 shows the resulting population factor c_p [cf. (10)] for the different flames and excitation lines. The dependence of c_p on flame type is quite obvious: The nitrogen-doped flame shows by far the largest signal from $v' = 0$, followed by the helium-doped and H_2/O_2 flames. This is consistent with the observation of Copeland et al. [6], according to which nitrogen is very efficient at VET, but a poor quencher. In contrast, water is rather inefficient at VET, but a fast quencher. A trend with the quantum number of the laser-excited level is obvious from the nitrogen-doped flame data: The relative population in $v' = 0$ diminishes with increasing N', indicating a decrease in VET efficiency for excitation of the higher-lying OH rotational levels. The same trend is also consistent with the data for the H_2/O_2 and helium-doped flames, but the associated error bars are too large to claim this with certitude.

2.4 Total removal rates

From the time-resolved signals of the $v' = 1$ state population, the value of τ_1^{-1} was determined by fitting a single exponential decay [cf. (6)] to the experimental curve for times later than the end of the laser pulse. Evaluation of the 1–1 band and 1–0 band data gave results that

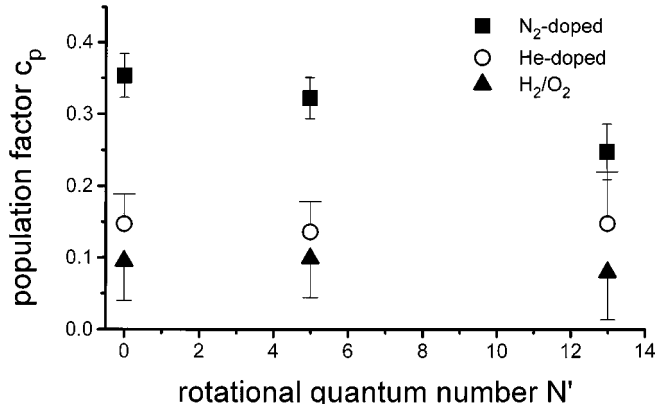

Fig. 5. Population ratio c_p [cf. (10)] for the three flames and laser-pumped levels

agreed within less than 3%. For determination of τ_0^{-1}, (7) was fitted to the time-resolved fluorescence signal of the 0–0 band. The previously determined value of τ_1^{-1} was used as an input parameter here. The error bar for τ_0^{-1} is larger, mostly because the difference between two large numbers enters its determination (cf. (7)). Table 2 summarizes these results in terms of total removal rates. Inspection of the data for $v' = 1$ and $v' = 0$ shows that in the H_2/O_2 flame, the effective lifetimes are a factor of 1.6 to 2 shorter than in the other flames, where the fast-quenching water was diluted. Also, $v' = 0$ is depopulated faster than the vibrationally excited state. Since in $v' = 1$ both quenching and VET contribute to the removal rate, this implies that quenching is slower in $v' = 1$ than in the vibrational ground state.

Now the rate V_{10} could, in principle, be deduced from (9) by inserting the values for c_p and τ_0^{-1}. A different approach was chosen for two reasons: the relatively large errors in τ_0^{-1} affect the result, and because of rotational relaxation within $v' = 1$, the effective VET rate will be slightly time-dependent. The procedure that was actually used was adapted from the RET work of [13, 23]. The right-hand side of (8) was plotted as a function of time; the integrals were evaluated numerically. Then, V_{10} was determined by extrapolating back to time $t = t_{\text{laser}}$, i.e. the start of the laser pulse. This procedure was originally developed to find RET rate coefficients under single-collision conditions. In our work it turned out to be less sensitive to errors in τ_0^{-1} than the

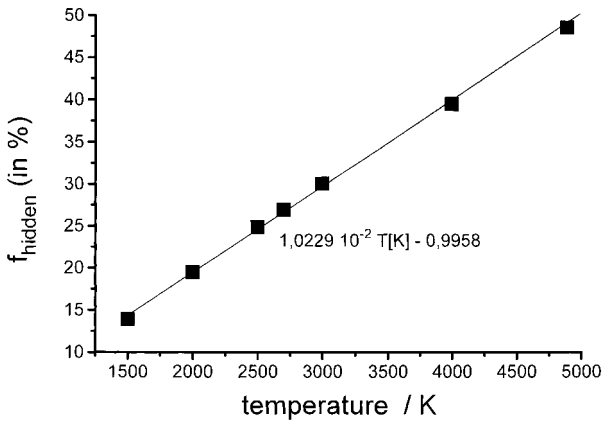

Fig. 4. Temperature dependence of f_{hidden}, the correction factor for spectral overlap. The measured integrated signal intensity in the non-overlapped 0–0 band region (306–312.2 nm) has to be incremented by this factor to obtain the "true" signal intensity for the 0–0 band [i.e. $I_{\text{true}} = I_{\text{meas}}(1 + f_{\text{hidden}})$]

Table 2. Total removal rates for $v' = 1$ and $v' = 0$ (in $10^6\,\mathrm{sec}^{-1}$) for the flames and excitation lines investigated

excitation line (in $v' = 1$)	removal rate: flame (temperature)	τ_1^{-1}	τ_0^{-1}	V_{10}
$P_1(1)$	H_2/O_2(1920 K)	123 ± 4.9	140 ± 14	13.1 ± 1.0
	He-doped(1520 K)	72 ± 2.9	75 ± 3.8	11.1 ± 0.67
	N_2-doped(1600 K)	74 ± 3.7	71 ± 4.3	24.3 ± 1.5
$Q_1(5)$	H_2/O_2	116 ± 7.0	134 ± 13	14.0 ± 0.98
	He-doped	66 ± 3.3	70 ± 7.0	9.5 ± 0.57
	N_2-doped	67 ± 3.4	66 ± 5.3	18.6 ± 1.3
$R_1(12)$	H_2/O_2	112 ± 7.8	120 ± 8.4	9.4 ± 0.66
	He-doped	62 ± 3.1	63 ± 3.2	7.5 ± 0.53
	N_2-doped	62 ± 2.8	58 ± 2.9	13.4 ± 0.80

simpler approach of (9), and to some extent the effect of rotational relaxation within $v' = 1$ on V_{10} should be reduced. The last column of Table 2 displays the resulting V_{10} for the three different flames. Comparison with the population factors c_p in Fig. 5 is instructive. It shows that the N_2-doped flame exhibits both the fastest total VET rate and the largest c_p factor. The He-doped flame, however, which shows a larger *signal* from $v' = 0$ than the H_2/O_2 flame, has the smallest *total* VET *rate*. This can be understood by considering flame compositions and relative efficiencies of collider species. In the He-doped flame, VET must stem mainly from the "residual" component and, to some extent, from water. Because the concentration of the fast quenching H_2O is reduced by more than a factor of 2 (cf. Table 1), the relatively smaller amount of OH that relaxes to $v' = 0$ has a much greater chance to fluoresce than in the H_2/O_2 flame.

2.5 Species-specific rate coefficients

Equations (3) to (5) link the total removal rates with concentrations and species-specific rate coefficients. In order to infer collider-specific coefficients from these rates, additional information concerning the contribution to quenching and VET by the other species in the flame is required. Reactive intermediates and unreacted educts form a "residual" component of the low-pressure flame which is unavoidably present in varying concentrations (cf. Table 1). Since experimental data for these species are not readily available, it is difficult to determine rate coefficients for the "residual" (see [8] for measured O_2 data and a literature compilation).

2.5.1 Quenching and VET coefficients for H_2O *and* N_2. Being a combustion product, water is always present in large quantities. Its concentration in a flame can not be varied beyond certain limits. Its contribution to the removal rates is therefore assessed first. The purpose of measuring in a helium-doped flame was to change the relative contributions of water and "residual" components by dilution with an inert gas, which is known to be extremely inefficient at both quenching [24] and VET [4] Two approaches for data evaluation were chosen.

In a first attempt, rate coefficients for quenching and VET by the "residual" components H_2, O_2, OH, H and O were calculated based on data from [8]. All coefficients there are given for 1900 K and $Q_1(5)$ excitation. For the following estimates, it was assumed that the cross sections do not depend on temperature for the range considered here (i.e. 1500–1900 K), hence the rate coefficients were scaled with a $\sqrt{T/T_0}$ dependence, with $T_0 = 1900$ K. The coefficients for $P_1(1)$ and $R_1(12)$ excitation were then scaled with a factor of 1.081 and 0.865, respectively; these factors were obtained by drawing an analogy between the N dependent quenching behaviour of water [25] and that of the "residual" components. Since a preliminary evaluation of our data showed that the quenching coefficient for H_2O was about 20% smaller in $v' = 1$ than in $v' = 0$, the "residual" coefficients for $v' = 1$ were in a first approximation scaled down by 20% for the final analysis. Furthermore, it was assumed that helium does not contribute to quenching or VET. Using the rate coefficients obtained with these assumptions, and the mole fractions calculated with the flame simulation code, quenching and VET coefficients for collisions with water could be deduced from the H_2/O_2 and helium-doped flames (cf. Table 3). If instead we use cross sections at the value for the $Q_1(5)$ excitation line given by Paul [8], k_{VET} is changed by about $0.2 \times 10^{-11}\,\mathrm{cm}^3\mathrm{sec}^{-1}$, which is well within the error bar. It is also important to note that the "residual" component contributions to the combined VET plus quenching in $v' = 1$ are only about 19% for the H_2/O_2 flame, 25% for the He-doped, and 27% for the N_2-doped flame. The corresponding "residual" contributions to quenching in $v' = 0$ are 10%, 14%, and 16%, respectively (the major uncertainty at this point is the contribution of the H atoms). So while the errors in estimating the "residual" rate coefficients are undoubtedly quite large, they will not propagate fully into the final results.

In the second approach, rate coefficients for the "residual" and water were evaluated without referring to literature values. It was again assumed that collisions with helium have no influence on VET and quenching. The H_2/O_2 and helium-doped flame gases consist essentially of water vapor and the "residual" components, with only their concentration ratio differing (cf. Table 1). Using (4), one can set up and solve a system of two equations (for the two flames) with the two VET rate coefficients (water and "residual") as unknowns. Similarly, (5) yields the two coefficients for quenching in $v' = 0$. Finally, (3) can be solved for the re-

Table 3. Rate coefficients for VET ($v' = 1 \rightarrow 0$) and quenching in $v' = 1$ and $v' = 0$ (in units of $10^{-11}\,\mathrm{cm}^3/\mathrm{molecule\,sec}$) for colliders H_2O and N_2 at 1600 K

excitation line (in $v' = 1$):	$P_1(1)$		$Q_1(5)$		$R_1(12)$	
$T = 1600$ K	H_2O	N_2	H_2O	N_2	H_2O	N_2
k_{VET}	1.03 ± 1.8	10.1 ± 2.0	1.05 ± 1.6	6.10 ± 1.8	-0.32 ± 1.4	3.81 ± 1.3
k_{Q_1}	59.1 ± 6.5	-4.1 ± 5.3	54.7 ± 6.4	-1.9 ± 5.4	54.9 ± 6.6	-0.71 ± 5.0
k_{Q_0}	74.6 ± 10.4	2.39 ± 7.9	70.6 ± 10.3	1.42 ± 8.2	63.4 ± 7.3	0.41 ± 5.7

maining two quenching coefficients for $v' = 1$. It is assumed here that the relative composition of "residual" compounds is the same in the H_2/O_2 and He flames. The composition of the helium-doped flame had been specially taylored to optimize this evaluation step, i.e. the concentration ratio of water to "residual" was reduced and the mole fraction of the "residual" was minimized. The amount of helium that can be added is limited by flame stability. This second procedure could, however, not improve on the error estimates and yielded essentially identical results. Therefore only the results of the first procedure are shown in Figs. 6 and 7 and Table 3.

Once the values for water are established, the rate coefficients for OH quenching and VET by nitrogen can be derived from the total removal rates in the nitrogen-doped flame. The N_2 rate coefficients and their associated error bars are slightly different, depending on which procedure was used for determining these water coefficients but the results are consistent. The "N_2" column of Table 3 shows the coefficients that were obtained when the H_2O data of the first approach was used.

2.5.2 Discussion and comparison with literature data. Figure 6 shows the quenching rate coefficients for $v' = 0$ and $v' = 1$, for colliders H_2O and N_2, at $T = 1600$ K (bars are 1σ error estimates). It is obvious that N_2 is a poor quencher.

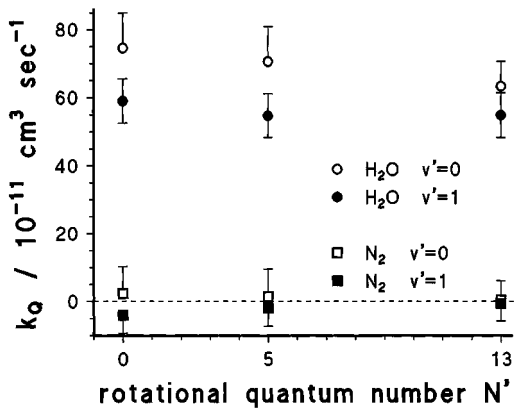

Fig. 6. Quenching rate coefficients (in 10^{-11} cm^{3}sec^{-1}) for H_2O and N_2 in $v' = 1$ and $v' = 0$ (excitation was to the $v' = 1$ level)

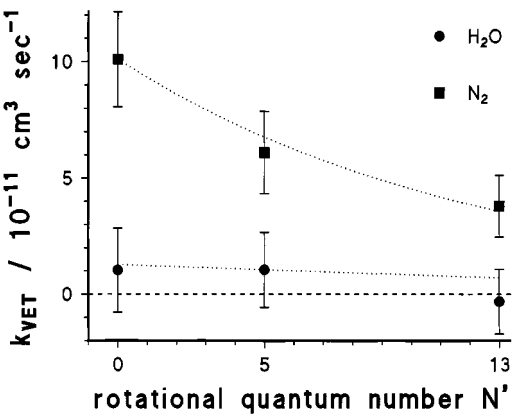

Fig. 7. VET rate coefficients (in -11 cm^{3}sec^{-1}) for H_2O and N_2 in $v' = 1$ and $v' = 0$. The dotted lines indicate the N' dependence employed in the LASKIN simulations

In $v' = 0$, the average value for the three excitation lines is 1.4×10^{-11} cm^{3}sec^{-1}, with an error estimate of the order of 7×10^{-11} cm^{3}sec^{-1}. In $v' = 1$, the average coefficient is even negative ($-2.2 \pm 5.2 \times 10^{-11}$ cm^{3}sec^{-1}), but the error estimate reaches far into the physically possible positive range.

Reference [24] compiled N_2 quenching data for $v' = 0$. At temperatures between 940 K and 1150 K, cross sections were reported that correspond to a rate coefficient between 0.85 and 1×10^{-11} cm^{3}sec^{-1}. In [14] the cross section at 1530 K was estimated to be 0.6 Å^2, corresponding to 1.2×10^{-11} cm^{3}sec^{-1}. For 1900 K, [8] gives quenching coefficients of 1.01 and 1.13×10^{-11} cm^{3}sec^{-1} for $v' = 0$ and $v' = 1$, respectively. For our conditions, the quenching contribution of N_2 is essentially zero. Quenching by H_2O is fast. For $v' = 1$, quenching coefficients between 59×10^{-11} cm^{3}sec^{-1} ($v' = 1$, $P_1(1)$ excitation) and 55×10^{-11} cm^{3}sec^{-1} ($v' = 1$, $R_1(12)$ excitation) were found, corresponding to cross sections between 30 and 27.9 Å^2. The N dependence is rather weak (8% decrease). The error estimates are 12% on average. In $v' = 0$, the coefficients fall in the range between 75×10^{-11} cm^{3}sec^{-1} ($v' = 1$, $P_1(1)$ excitation) and 63×10^{-11} cm^{3}sec^{-1} ($v' = 1$, $R_1(12)$ excitation), corresponding to cross sections between 37.9 and 32.2 Å^2. The level dependence shows a 15% decrease from $N' = 0$ to 13, and the error estimate is 13% on average.

For OH in $v' = 1$, [25] determined the N dependence of H_2O quenching cross sections at $T = 1048$ K, for $N' = 4$ to 11. They found a 16% decrease over this range, corresponding to $(51–43) \times 10^{-11}$cm^{3}sec^{-1}. For OH in $v' = 0$, Paul [24] calculated the temperature dependence of the H_2O quenching cross section with a "harpooning" model. In his Fig. 4, his calculated curve is compared with experimental results between 300 K and 2300 K. In general, the agreement between the "harpooning" model and experimental data is quite reasonable. More recently, Kienle et al. [14] estimated a cross section of 29 Å^2 at 1530 K for $N' = 5$, $v' = 0$, corresponding to 56×10^{-11} cm^{3}sec^{-1}. The rotational level dependence of quenching was investigated for several flame temperatures between 1200 K and 2300 K in [26]. It was found that the level dependence diminishes with increasing temperature and has almost vanished at 2300 K. In [15] quenching rates for level-specific excitation in $v' = 0$ were measured in a 25 mbar H_2/O_2/He flame at 1330 K, where most of the quenching can be attributed to water. The total quenching rates unambiguously showed a decrease of about 18% between $N' = 0$ and 15. Using the LASKIN code, these data were further analyzed in [14] to assess the influence of RET on the experimentally accessible quenching rates. Briefly, RET tends to average out the N dependence of the truly level-specific quenching coefficients, thus producing a reduced slope of the experimentally determined dependence even if state-selective excitation is used. Two effects cooperate to amplify this trend: Higher temperatures will accelerate RET and tend to average out the different level-specific quenching coefficients. Also, the N dependence of these coefficients becomes weaker at higher temperatures. One can see now how the H_2O quenching coefficients for $v' = 1$ from this work fit into the generally observed trends. The only high-temperature value to compare with is from [25]. If their cross section for $N' = 5$ is scaled with temperature according to the "harpooning" model curve in [24] (which was calculated for $v' = 0$), their value agrees with the coefficient found in this

work within the error limits. The rotational level dependence found in [25] is steeper than what was observed in this work; this can be expected from the above considerations [14, 26].

In the discussion of the coefficients for $v' = 0$ it should be kept in mind that in this work, quenching for $v' = 0$ is measured after laser excitation to $v' = 1$, i.e. in a rather indirect fashion. The determination of the total removal rate τ_0^{-1} was already hampered by a relatively large error (cf. Sect. 2.4 above). And because of the sequence of collision processes consisting of level-specific excitation $\rightarrow$ RET within $v' = 1 \rightarrow$ VET $\rightarrow$ RET within $v' = 0$, the rotational population distribution in $v' = 0$ will be rather different compared to the case of exciting a specific level in $v' = 0$ directly. The apparent, indirectly determined quenching coefficients reported in this work are somewhat high, $(71 \pm 10) \times 10^{-11}$cm^{3}sec^{-1} ($v' = 1$, $Q_1(5)$ excitation), compared with a value of $\approx 51 \times 10^{-11}$ cm^{3}sec^{-1} (=26 Å^2) for $T = 1600$ K inferred from the calculated curve in [24], and 56×10^{-11} cm^{3}sec^{-1} (= 29 Å^2) at 1530 K in [14].

The VET rate coefficients for H_2O and N_2 are displayed in Fig. 7. The H_2O coefficients are very small (with an average value of $0.59 \pm 1.6 \times 10^{-11}$ cm^{3}sec^{-1}). The rate coefficients for N_2 are much larger and exhibit a pronounced N dependence. They range from 10.1×10^{-11} cm^{3}sec^{-1} ($N' = 0$) to 3.8×10^{-11} cm^{3}sec^{-1} ($N' = 13$).

Literature data for VET with water is available in [6]. These authors found, at room temperature, an upper limit of 12×10^{-11} cm^{3}sec^{-1} for $N' = 5$. In a very recent publication reporting on measurements in a discharge flow reactor at ambient temperature [7], this upper limit was replaced by $7.3 \pm 0.5 \times 10^{-11}$ cm^{3}sec^{-1}. In [25] it was concluded that the VET contribution of H_2O in a low-pressure $H_2/O_2/Ar$ flame ($T \approx 1048$ K) is negligible. This conclusion is confirmed by the results presented here. The VET coefficient for nitrogen was repeatedly measured at room temperature (see e.g. [2, 4, 5, 26]). The results for 300 K are in the range (10 to 28)$\times 10^{-11}$cm^{3}sec^{-1} for various initial levels. A study at elevated temperature [8] for $N' = 5$ yielded a rate coefficient of 7.02×10^{-11} cm^{3}sec^{-1} at 1900 K and 7.32×10^{-11} cm^{3}sec^{-1} at 2300 K. The latter values, when scaled with $\sqrt{T}$, compare very favorably with our coefficient of 6.1×10^{-11} cm^{3}sec^{-1} at 1600 K. To our knowledge, the N dependence for nitrogen VET was previously determined at room temperature only. A decrease by a factor of seven was observed between $N' = 0$ and $N' = 13$ in [4]. In [5], the coefficient dropped from 25.9×10^{-11} cm^{3}sec^{-1} to 16.9×10^{-11} cm^{3}sec^{-1} between $N' = 0$ and $N' = 5$. Since the N dependence of collision processes tends to be less pronounced at higher temperatures, the decrease found in this work (a factor of 2.7 for $N' = 0$ to $N' = 13$) is certainly in a reasonable range.

To summarize briefly: The previously found trends regarding efficiency at quenching and VET for water and nitrogen can be confirmed for the flame temperatures encountered in this study – N_2 is a poor quencher, but an efficient collider for VET; the reverse holds for H_2O. To our knowledge, these measurements are the first attempts to determine k_{VET} for water at flame temperatures. For nitrogen, measurement of three initially pumped levels showed that the N dependence of k_{VET} persists also at flame temperatures.

2.6 Modeling of state-to-state-specific VET coefficients

Our analysis has now proceeded from determination of total removal rates (which can be derived quite unambiguously from the decay curves, cf. Sect. 2.2) to the extraction of collider-specific rate coefficients (which involves quite a few assumptions regarding the scaling and extrapolation of existing data on quenching and VET). Since our numerical model requires an input of state-to-state-specific rate coefficients, we now have to move one step further to discuss this problem. In principle, the VET step must take place between two well-defined rotational states of the OH radical. The coefficients available from our experiments are specific with regard to the initially laser-populated rotational level, but not with regard to the final level. They rather represent a weighted sum of state-to-state coefficients.

It is important to know state-to-state-specific values both for a more thorough understanding of the vibrational relaxation process and for our modeling purposes. Without additional experimental data, however, an element of speculation will necessarily be involved in any attempt to decompose the collider-specific coefficients determined above into state-specific coefficients. The major justification for such an attempt will stem from the (partial) success in reproducing features of the original experimental data. From inspection of the LIF spectra presented in Sect. 2.1, the ability to reproduce the overall shape of the spectral signature lends itself as one point that can be used to judge the merits of a particular model assumption. Also, the observable trend of the apparent rotational temperature for the 0-0 band (cf. Sect. 2.3) can be employed to discriminate between different suggestions.

Detailed modeling of state-to-state dynamics in the electronically excited A state of OH provides a very helpful tool both for the quantitative analysis and interpretation of experimental data, and (perhaps even more important) for identification of experimental approaches that are suitable for a given measurement task. Within a kinetic rate equations framework, the LASKIN code described in [13, 14] (see also [27] for details of the differential equation solver used) calculates time-dependent populations in the individual OH rotational states, i.e. rotational relaxation (RET), quenching, stimulated and spontaneous emission after excitation to a specific level. It also simulates spectrally or temporally resolved LIF signals for direct comparison with experimental data. In the course of the present work, this LASKIN code was extended to include vibrational energy transfer between the $v' = 1$ and $v' = 0$ vibrational levels. At the same time, the code was transferred from PC to the workstation level and translated to the "C" programming language, which greatly increased the speed of calculations. At present, approximately 80 molecular energy levels are treated simultaneously. For each rotational-vibrational level, the differential equation describing its time dependent population was extended to include a VET term. The necessary rate coefficients were mostly taken from the previous [14] program version (Einstein A and B coefficients, RET coefficients as modeled by an "energy corrected sudden" scaling relationship [22], and quenching coefficients). The VET coefficients were obtained from the experiments described in this work. Their temperature dependence was scaled with $\sqrt{T/T_0}$. The N dependence was approximated as $k_{VET}(N)/k_{VET}(0) = 1 - 0.0343 \times N$ for water, and as an exponential function: $k_{VET}(N)/k_{VET}(0) = \exp(-0.08 \times N)$ for

nitrogen (the dotted lines in Fig. 7 indicate the resulting slopes). In a first application of the extended program version, LIF spectra and time-resolved signals were simulated for testing the data evaluation procedure described in Sect. 2.4. It was found that the procedure correctly retrieves the parameters used in the simulations. In the worst case studied, a 6% relative error in k_{VET} resulted, which is small compared to the error limits encountered in the experimental data evaluation.

For decomposing the measured total VET coefficient into state-to-state-specific values, a choice has to be made for the rotational dependence of this relation. To our knowledge, a theoretical selection rule for this problem is not available; so a set of ad hoc model assumptions was tested in the simulation of the experimental LIF spectra. At this stage it becomes necessary to allow for a distinction between the F_1 and F_2 doublet components, hence the rotational quantum number $J(= N \pm 0.5)$ is introduced.

Figure 8 illustrates the models tested for the extraction of state-specific coefficients. Line thickness of the arrows is meant to indicate different transition probabilities. In all models, transitions from a given initial state were permitted only to a final state that was lower in energy. The first assumption was a simple conservation of rotational quantum number J (including spin). The second assumption was that a given initial level will populate all levels in $v' = 0$ with equal probability, regardless of spin. The third assumption was that the transition probability scales with the degeneracy $(2J_{\mathrm{final}} + 1)$ of the final level in $v' = 0$, considering the number of possible channels for this transition. This implies that the rotationally highly excited levels in $v' = 0$, which are energetically closer to the $v' = 1$ state, are preferentially populated.

Note that as soon as an OH molecule has undergone VET into $v' = 0$, rotational relaxation sets in and tends to establish an equilibrium distribution, in competition with emission and quenching processes. The three assumptions differ in the shape of the original distribution in $v' = 0$ that forms the starting point for this process. Figure 9 illustrates this point; it shows the time-integrated population in the $v' = 0$ level for the three model assumptions, after excitation of the $Q_1(5)$ line. The RET efficiency in $v' = 0$ was arbitrarily reduced to 10% of its correct value to make the differences more clearly visible. The simulation for the first assumption (J conservation) is plotted in diagram a (for the F_1 levels) and b (F_2). The

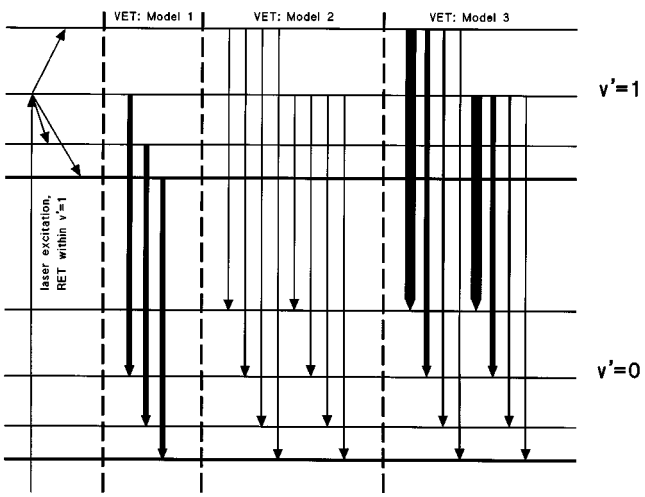

Fig. 8. Model assumptions for rotational-level-dependence of state-specific rate coefficients. Leftmost column: Laser excitation and RET within $v' = 1$. Model 1: VET populates only level with same rotational quantum number. Model 2: VET populates all rotational levels in $v' = 0$ with equal probability. Model 3: VET populates all rotational levels in $v' = 0$, but probability is weighted with the degeneracy factor $(2J_{\mathrm{final}} + 1)$. The arrow thicknesses indicate different probabilities of the VET step

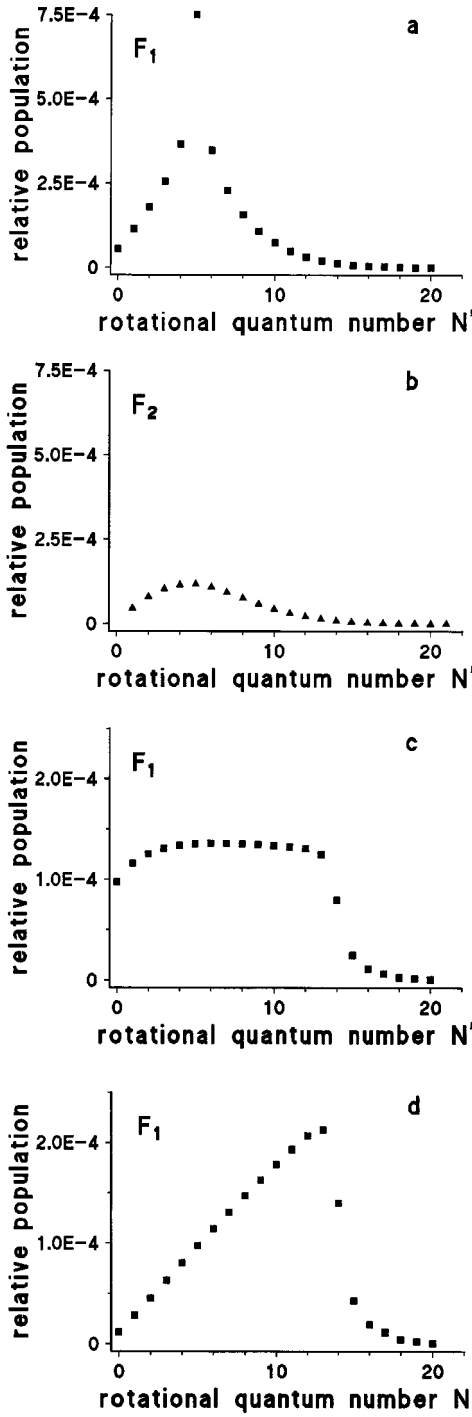

Fig. 9a–d. Time-integrated population in $v' = 0$ for the three VET model assumptions. The RET within $v' = 0$ was reduced to 10% of its correct value to enhance visibility of differences. Panels (**a**) and (**b**) : Model assumption 1, for F_1 levels (a) and F_2 levels (b) separately. Panel (**c**) : Assumption 2, only F_1 levels shown; panel (**d**) : Assumption 3, also only F_1 levels shown

laser-excited level ($N = 5$) stands out clearly, but the neighbours are already populated to some extent, mostly because of RET in $v' = 1$ (which was left at the correct value). Note that equilibration between the F_1 and F_2 levels is drastically reduced in comparison with the other two assumptions. In panel c, the simulation assumed equally probable transfer to all levels in $v' = 0$, and only the F_1 level populations are shown (the F_2 levels show almost identical behaviour). The sharp fall-off around $N' = 14$ is caused by the restriction to exoergic transfer steps. Levels in $v' = 0$ higher than $N' = 13$ can then only be populated by RET within $v' = 0$ or by a VET process from a high rotational level in $v' = 1$. Note also that for the levels with low N' the population is reduced faster than for those with intermediate N', because the RET coefficients are largest for low N'. In panel d, assumption 3 [transfer probability scaling with $(2J_{\text{final}} + 1)$] was used for the calculation, and again only the F_1 level populations are shown. Obviously, the high-lying levels are then populated preferentially. As to the fall-off at $N' = 14$, the same considerations as for panel c apply; but the reduced population at low N' can be seen on a logarithmic scale only.

Based on these three ad hoc assumptions, spectra were calculated for the flame conditions and excitation lines employed in the experiments. Results of these simulations are discussed for the nitrogen-doped flame, where VET is strongest, and the signal-to-noise of the experimental spectra is best. Not surprisingly, none of the three model assumptions is perfect. Table 4 compares the apparent temperatures of the experimental $v' = 0$ band spectra with the temperatures resulting from the simulations. In Fig. 10, a section of the experimental spectrum in the 0–0 band for $Q_1(5)$ excitation is shown (trace b), together with two curves calculated with the model assumptions. The first assumption (J conservation – trace a) definitely fails in reproducing the rather high apparent temperature in $v' = 0$ (2500 K). Note also the clear discrepancies of amplitude ratios in the 308–309 nm range. Also, the error sum of squared deviations is much higher for this assumption than for the other two. The second assumption (equally probable transfer, not shown in Fig. 10) yields lower error sums; the apparent temperature is ≈ 1850 K, but is almost independent of the excitation line, which is in contrast with the experimental findings. The third assumption (scaling with $(2J_{\text{final}} + 1)$ – trace c) yields the lowest error sums, and the apparent temperatures show a trend from ≈ 2700 K for the $P_1(1)$ excitation line to 2850 K [$Q_1(5)$] and 3300 K [$R_1(12)$].

Table 4. Comparison between different VET simulation models. Second column: The apparent rotational temperature extracted from the experimental 0–0 band spectra (cf. Sect. 2.3). Columns 3 to 5: Best-fit rotational temperatures for the same wavelength interval of the simulated spectra; enclosed in brackets are the error sums

excitation line	experimental	model 1	model 2	model 3
$P_1(1)$	2150 K	< 1000 K (0.272)	1800 K (0.065)	2700 K (0.075)
$Q_1(5)$	2500 K	1300 K (0.266)	1850 K (0.101)	2850 K (0.074)
$R_1(12)$	4900 K	2750 K (0.135)	1850 K (0.128)	3300 K (0.071)

It can be concluded that the first assumption - conservation of rotational quantum number J during VET - is inappropriate for this system. While this result may sometimes be guessed from inspection of the spectrally resolved fluorescence, it should be kept in mind that rotational relaxation in $v' = 1$ and $v' = 0$ may be capable of disguising such a preference. The third assumption yields spectra with apparent temperatures that show the same trend as, though not quantitative agreement with, the experimental data. The second assumption yields fits to the experimental spectra which have about 20% higher sum-of-squares errors, and the apparent temperatures do not show the observed trend.

An obvious shortcoming of the model assumptions discussed in this paragraph is the lack of a sound physical picture behind them. Clearly, theoretical efforts are required to shed more light on this particular subject. But, as was pointed out above, for the time being these model assumptions may serve the purpose of providing input data for a numerical code for the simulation of OH population dynamics.

3 Summary

Vibrational relaxation and quenching of OH by collisions with water and nitrogen were measured in a low-pressure flame. For three initially laser-populated rotational levels in $v' = 1$, total removal rates for $v' = 1$ and $v' = 0$ were de-

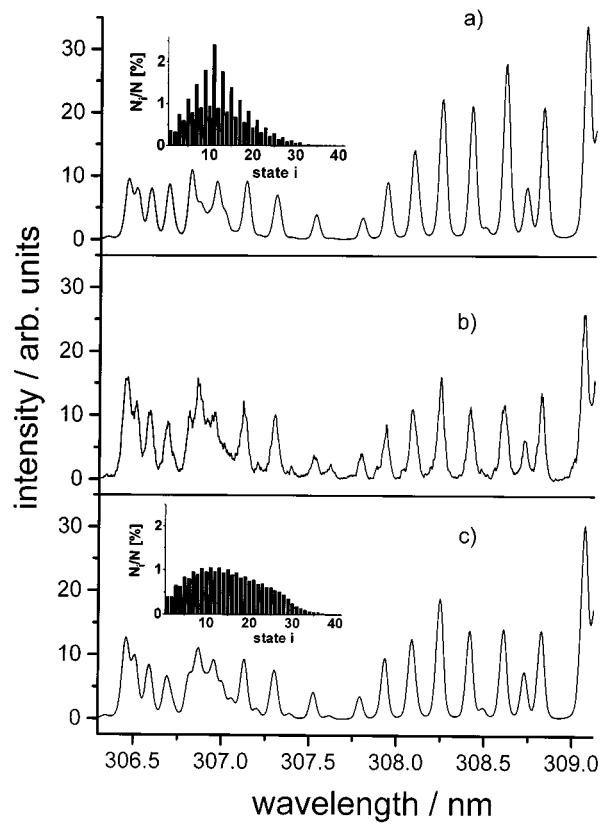

Fig. 10. Comparison between experimental LIF spectrum (trace (**b**): N_2-doped flame, $N' = 5$ excitation) and two simulations. Trace (**a**): Calculated with model assumption 1. Trace (**c**): Calculated with model assumption 3. The inserts show time-integrated rotational level populations in $v' = 0$, with F1 and F2 levels alternating

termined from time-resolved fluorescence signals. With the calculated flame composition and literature VET and quenching rate coefficients for minor species in the flame, a set of species-specific coefficients for quenching and VET was then derived. A second method for evaluating species-specific coefficients, which makes use of composition differences between a "pure" H_2/O_2 flame and a helium-doped flame, was also tested. Under the given circumstances, its results were more susceptible to errors and were not used in the further analysis.

The resulting rate coefficients for VET fit into the general picture which emerged over the last few years: N_2 is a poor quencher; within the error limits, its contribution in the flame can be set equal to zero. Nitrogen is, however, a main contributor to vibrational relaxation in the flame. In our measurements, a marked N dependence for this VET coefficient was noted. Water behaves in the opposite way; its contribution to VET is close to zero also at flame temperatures, but it is a very efficient quencher.

A kinetic model for the simulation of population dynamics in the OH A state was extended to include VET between $v' = 1$ and $v' = 0$. Various assumptions for state-to-state-specific VET rate coefficients were tested. According to these simulations, the VET step occurs without noticeable conservation of angular momentum for the OH molecule. The model which is most successful in reproducing the experimental spectra assumes a wide distribution of final states from a given level in $v' = 1$, biased towards high J_{final} values.

The needs for future work can be divided into the categories of experimental advances and theoretical efforts. A logical extension of the experimental work described in this paper will be the use of a shorter-pulse laser in conjunction with a detection system that has better time resolution, e.g. a streak camera. The simultaneously time- and wavelength-resolved signal should facilitate the analysis of the population dynamics. Also, measurements with other colliders of importance in flames are needed (CO_2 as a major product of hydrocarbon combustion is an obvious candidate).

On the theoretical side, a point of great interest should be the calculation of state-to-state-specific cross sections from an interaction potential for an OH-collider system which takes rotational quantum states into account. Calculations for the triatomic, non-linear H_2O molecule as collider species would perhaps be the most challenging task. From such calculations one may hope to find appropriate guidelines for selection rules, relative probabilities and dependence on temperature and quantum state for the scaling behaviour of the various collision processes. It may be noted here that knowledge of the collisional relaxation behaviou should also be useful for the quantitative interpretation of resonant four-wave mixing spectroscopy data (cf. [28]). A detail of the RET modeling also deserves further attention: During the relaxation in $v' = 0$, very high rotational levels are involved. It may not be taken for granted that the ECS scaling law, which was developed from a data base measured at low to medium temperatures, can be reliably extrapolated to the high temperatures and rotational levels (say, $N' > 15 - 20$) involved in the VET step in flames.

Acknowledgements. The authors are grateful to J. Heinze and A.O. Vyrodov for providing a temperature fit routine for OH, and to J. Luque and D.R. Crosley for a copy of their LIFBASE spectra calculation software. They acknowledge fruitful discussions with M.P. Lee, who also assisted in the laboratory in the initial phase of this work. LASKIN in the state of evaluation described in [14] was developed at DLR Stuttgart; it is available there. Details regarding the model and its present shape may be obtained from the authors (E-mail to KKH@CHEP118.UNI-BIELEFELD.DE).

References

1. K. Kohse-Höinghaus: Prog. Energy Combust. Sci. **20**, 203 (1994)
2. R.K. Lengel, D.R. Crosley: Chem. Phys. Lett. **32**, 261 (1975)
3. K.R. German: J. Chem. Phys. **64**, 4065 (1976)
4. R.K. Lengel, D.R. Crosley: J. Chem. Phys. **68**, 5309 (1978)
5. J. Burns, J.J. Butler, T.J. McGee, W.S. Heaps: Chem. Phys. **124**, 251 (1988)
6. R.A. Copeland, M.L. Wise, D.R. Crosley: J. Phys. Chem. **92**, 5710 (1988)
7. L.R. Williams, D.R. Crosley: J. Chem. Phys. **104**, 6507 (1996)
8. P.H. Paul: J. Phys. Chem. **99**, 8472 (1995)
9. J.W. Daily: Appl. Opt. **16**, 2322 (1977)
10. C. Chan, J.W.Daily: Appl. Opt. **19**, 1357 (1980)
11. D.H. Campbell: Appl. Opt. **23**, 689 (1984)
12. R.P. Lucht, D.W. Sweeney, N.M. Laurendeau: Appl. Opt. **25**, 4086 (1986)
13. R. Kienle: Ph. D. Dissertation, Universität Bielefeld (1994)
14. R. Kienle, M.P. Lee, K. Kohse-Höinghaus: Appl. Phys. B **62**, 583 (1996)
15. M.P. Lee, R. Kienle, K. Kohse-Höinghaus: Appl. Phys. B **58**, 447 (1994)
16. G.H. Dieke, H.M. Crosswhite: J. Quant. Spectrosc. Radiat. Transfer **2**, 97 (1962)
17. R.J. Kee, J.F. Grcar, M.D. Smooke, J.A. Miller: SANDIA Report SAND85-8240 (1985); Mechanism GRI-Mech: *An Optimized Kinetics Model for Natural Gas Combustion*: M. Frenklach, H. Wang, C.T. Bowman, R.K. Hanson, G.P. Smith, D.M. Golden, W.C. Gardiner, V. Lissianski: 25th International Symposium on Combustion, Irvine CA, Poster No. WIP-26 (1994)
18. P.H. Paul, J.L. Durant, Jr., J.A. Gray, M.R. Furlanetto: J. Chem. Phys. **102**, 8378 (1995)
19. J. Luque, D.R. Crosley (SRI): LIFBASE v0.99 spectra simulation code, private communication (1994)
20. J. Heinze, A.O.Vyrodov (DLR Stuttgart): private communication (1995)
21. M.R. Trolier: Ph. D. Thesis, Cornell University (1988)
22. R. Kienle, M.P. Lee, K. Kohse-Höinghaus: Appl. Phys. B **63**, 403 (1996)
23. A. Jörg, U. Meier, K. Kohse-Höinghaus: J. Chem. Phys. **93**, 6453 (1990)
24. P.H. Paul: J. Quant. Spectrosc. Radiat. Transfer **51**, 511 (1994)
25. R.J. Cattolica, T.G. Mataga: Chem. Phys. Lett. **124**, 251 (1991)
26. J.P. Jeffries, K. Kohse-Höinghaus, G.P. Smith, R.A. Copeland, D.R. Crosley: Chem. Phys. Lett. **152**, 160 (1988)
27. P. Deufihard, G. Bader, U. Nowak: In *Modeling of Chemical Reaction Systems* (K.H. Ebert, P. Deuflhard, W. Jaeger, eds), Springer Ser. Chem. Phys. **18**, pp. 38–55 (1981)
28. S. Williams, L.A. Rahn, R.N. Zare: J. Chem. Phys. **104**, 3947 (1996)